



Cite this: DOI: 10.1039/c6sc04797a

# Pyroglutamate-modified A $\beta$ (3-42) affects aggregation kinetics of A $\beta$ (1-42) by accelerating primary and secondary pathways†

C. Dammers,<sup>a</sup> M. Schwarten,<sup>a</sup> A. K. Buell<sup>b</sup> and D. Willbold<sup>\*ab</sup>

The aggregation into amyloid fibrils of amyloid- $\beta$  (A $\beta$ ) peptides is a hallmark of Alzheimer's disease. A variety of A $\beta$  peptides have been discovered *in vivo*, with pyroglutamate-modified A $\beta$  (pEA $\beta$ ) forming a significant proportion. pEA $\beta$  is mainly localized in the core of plaques, suggesting a possible role in inducing and facilitating A $\beta$  oligomerization and accumulation. Despite this potential importance, the aggregation mechanism of pEA $\beta$  and its influence on the aggregation kinetics of other A $\beta$  variants have not yet been elucidated. Here we show that pEA $\beta$ (3-42) forms fibrils much faster than A $\beta$ (1-42) and the critical concentration above which aggregation was observed was drastically decreased by one order of magnitude compared to A $\beta$ (1-42). We elucidated the co-aggregation mechanism of A $\beta$ (1-42) with pEA $\beta$ (3-42). At concentrations at which both species do not aggregate as homofibrils, mixtures of pEA $\beta$ (3-42) and A $\beta$ (1-42) aggregate, suggesting the formation of mixed nuclei. We show that the presence of pEA $\beta$ (3-42) monomers increases the rate of primary nucleation of A $\beta$ (1-42) and that fibrils of pEA $\beta$ (3-42) serve as highly efficient templates for elongation and catalytic surfaces for secondary nucleation of A $\beta$ (1-42). On the other hand, the addition of A $\beta$ (1-42) monomers drastically decelerates the primary and secondary nucleation of pEA $\beta$ (3-42) while not altering the pEA $\beta$ (3-42) elongation rate. In addition, even moderate concentrations of fibrillar A $\beta$ (1-42) prevent pEA $\beta$ (3-42) aggregation, likely due to non-reactive binding of pEA $\beta$ (3-42) monomers to the surfaces of A $\beta$ (1-42) fibrils. Thus, pEA $\beta$ (3-42) accelerates aggregation of A $\beta$ (1-42) by affecting all individual reaction steps of the aggregation process while A $\beta$ (1-42) dramatically slows down the primary and secondary nucleation of pEA $\beta$ (3-42).

Received 28th October 2016  
Accepted 3rd May 2017

DOI: 10.1039/c6sc04797a

rsc.li/chemical-science

## Introduction

Extracellular insoluble fibrillar structures are a pathological hallmark of Alzheimer's disease (AD) and are mainly composed of depositions of amyloid- $\beta$  peptides (A $\beta$ ).<sup>1,2</sup> Several A $\beta$  variants have been found in *in vivo* deposits, with N-terminally truncated A $\beta$  variants as a significant proportion.<sup>3,4</sup> Pyroglutamate-modified A $\beta$  (pEA $\beta$ ) variants, especially pEA $\beta$ (3-42), have been demonstrated to be the predominant isoforms amongst these.<sup>5-7</sup>

Modification to pEA $\beta$  results in altered biophysical and biochemical characteristics with potentially severe pathological consequences. Formation of the intramolecular lactam ring increases its resistance to degradation by amino peptidases and therefore the overall stability.<sup>8</sup> Since the modification to pEA $\beta$ (3- $x$ ) results in the loss of one positive and two negative charges, the enhanced hydrophobicity and decreased electrostatic

repulsion of pEA $\beta$ (3- $x$ ) leads to dramatically accelerated aggregation kinetics compared to A $\beta$ (1- $x$ ) – independently of the C-terminal length.<sup>9</sup> Structural analysis on pEA $\beta$ (3-40/42) and A $\beta$ (1-40/42) isoforms using solution state nuclear magnetic resonance (NMR) spectroscopy indicate that the pyroglutamate-modified variants have an increased tendency to form  $\beta$ -sheet rich structures compared to their non-truncated isoforms.<sup>10,11</sup>

Levels of pEA $\beta$  ending with position 42 were found to be always higher than C-terminally shortened species;<sup>4,12</sup> pEA $\beta$ (3-42) represents 25% of the total A $\beta$  in senile plaques.<sup>4</sup> Moreover, pEA $\beta$ (3- $x$ ) was detected in the core of amyloid aggregates *in vivo*, leading to the hypothesis that pEA $\beta$  deposition plays a central role in initiating the aggregation of full-length A $\beta$ .<sup>7,13-15</sup> In general, pEA $\beta$  was shown to be more likely to form  $\beta$ -sheet structures and has an enhanced aggregation propensity compared to the not N-terminally truncated peptide underlining its potential role in seeding A $\beta$  oligomerization and accumulation.<sup>9,16-18</sup> The N-terminus plays an important role in determining the thermodynamic stability of the fibrils<sup>19</sup> and the pEA $\beta$ (3- $x$ ) variants have been proposed to lead to enhanced fragmentation.<sup>20</sup> The increased aggregation propensity is in line with the hypothesis that pEA $\beta$ (3-42) fibrils act as a template for full-length A $\beta$  species.

<sup>a</sup>Institute of Complex Systems (ICS-6) Structural Biochemistry, Forschungszentrum Jülich, 52425 Jülich, Germany. E-mail: d.willbold@fz-juelich.de

<sup>b</sup>Institut für Physikalische Biologie, Heinrich-Heine-Universität Düsseldorf, 40225 Düsseldorf, Germany

† Electronic supplementary information (ESI) available. See DOI: 10.1039/c6sc04797a



As a major species in diffuse and compacted plaques in the human AD brain, pEA $\beta$ (3-42) is consequently an emerging target for active as well as passive immunotherapy trials.<sup>21</sup> Non-truncated A $\beta$ (1-40/42) are physiologically generated as products of normal APP turnover<sup>22,23</sup> whereas the occurrence of a significant proportion of pEA $\beta$ (3-40/42) is the result of a side reaction of the enzyme glutaminyl cyclase (QC) and alters the amyloidogenicity and toxicity of the A $\beta$  molecule.<sup>21</sup> Thus, new immunotherapy strategies focus on A $\beta$  peptides with high toxic potential such as pEA $\beta$ (3-40/42).<sup>24</sup> Although the detailed aggregation mechanism and the influence of pEA $\beta$ (3-42) on the kinetics of other A $\beta$  variants are still unknown, the aggregation mechanism of the unmodified A $\beta$ (1-42) peptide has been analysed in detail. Using a combination of kinetic experiments and theoretical analysis, it was demonstrated that A $\beta$ (1-42) aggregation is dominated by autocatalytic secondary nucleation under quiescent conditions.<sup>25–27</sup> Furthermore, it was shown that A $\beta$ (1-42) and its C-terminally truncated version A $\beta$ (1-40) do not significantly co-aggregate.<sup>28</sup> Interestingly, the insertion of N-terminal extensions of A $\beta$ (1-42) allows cross-seeding and co-aggregation<sup>29</sup> indicating that the presence of N-terminally modified forms of the peptide can have a strong effect on the aggregation kinetics of the full-length sequence.

In the present study, we have elucidated the co-aggregation mechanism of A $\beta$ (1-42) with the more toxic and aggregation prone variant pEA $\beta$ (3-42) by kinetic studies using highly pure recombinant peptides.<sup>30</sup>

## Results and discussion

### pEA $\beta$ (3-42) aggregation kinetics indicate increased secondary pathways

The aggregation kinetics of pure samples of pEA $\beta$ (3-42) and A $\beta$ (1-42) were monitored by Thioflavin-T (ThT) fluorescence. Theoretical analysis of aggregation kinetics was performed using the software AmyloFit.<sup>31</sup> First, we performed kinetic experiments of both A $\beta$ (1-42) and pEA $\beta$ (3-42) at various concentrations and found that pEA $\beta$ (3-42) aggregates much faster than A $\beta$ (1-42). Furthermore, the concentration above which aggregation was observed within the timescale of our experiments was decreased by one order of magnitude for pEA $\beta$ (3-42) compared to A $\beta$ (1-42) (Fig. 1A and B). While A $\beta$ (1-42) assembles into networks of long thin fibrils, pEA $\beta$ (3-42) fibrils are on average much shorter (Fig. 1C and D). This could be either caused by a higher fragmentation rate, as proposed recently,<sup>20</sup> or alternatively by a higher nucleation rate, with both scenarios leading to the formation of more, but shorter aggregates from a given initial concentration of monomeric peptide.<sup>32</sup>

The scaling exponents from a log–log plot of half time against initial peptide concentration are in both cases close to  $-0.5$  ( $-0.63$  for pEA $\beta$ (3-42) and  $-0.76$  for A $\beta$ (1-42)) (Fig. S1†), which is indicative of either a fragmentation dominated mechanism,<sup>33</sup> or of a saturated secondary nucleation mechanism.<sup>34</sup> It has previously been shown that the surface-catalysed secondary nucleation mechanism of the A $\beta$ (1-40) peptide becomes with increasing initial peptide concentration successively less concentration dependent as the binding sites on the

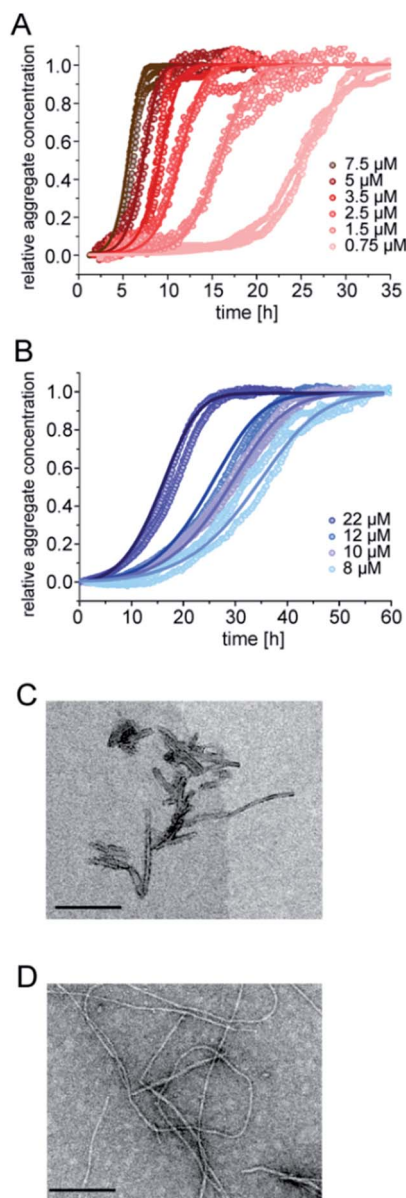
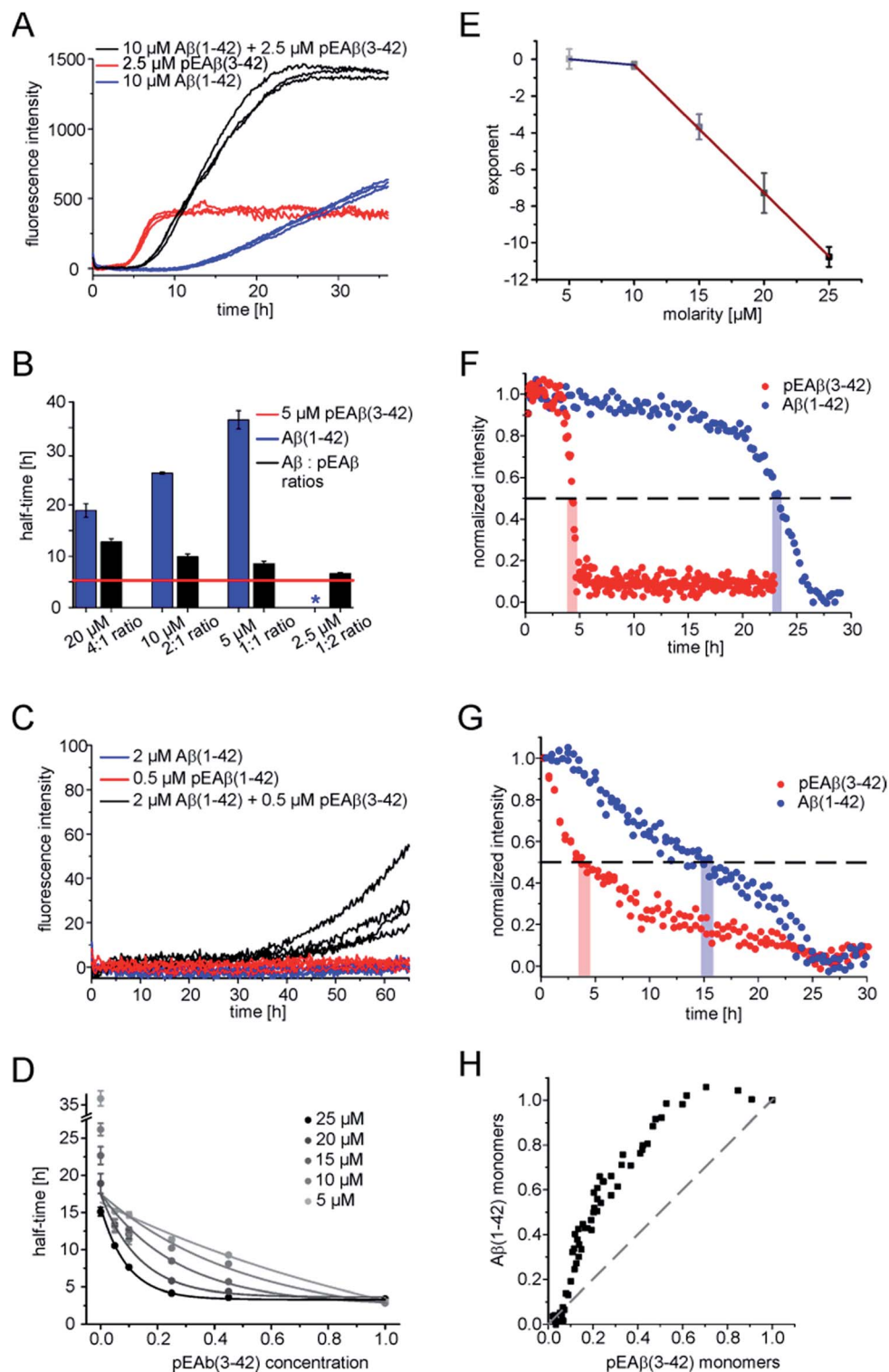


Fig. 1 Aggregation kinetics of A $\beta$ (1-42) and pEA $\beta$ (3-42) and TEM images of fibrils. Aggregation kinetics of pEA $\beta$ (3-42) (A) and A $\beta$ (1-42) (B) monitored by ThT fluorescence. Analysis was performed using the software AmyloFit<sup>31</sup> after normalizing the raw data according to their initial peptide monomer concentration. TEM images of pEA $\beta$ (3-42) (C) and A $\beta$ (1-42) (D) were obtained after seven days of incubation (the black scale bar corresponds to 200 nm).

surface of the fibrils become saturated at concentrations above *ca.* 10  $\mu$ M.<sup>34</sup> Our results are consistent with this picture, given that we are exploring a concentration range of 8–22  $\mu$ M in the case of the A $\beta$ (1-42) peptide. The finding that the scaling exponent of pEA $\beta$ (3-42) is lower than that for A $\beta$ (1-42) peptide, despite the fact that the experiments with the former were performed at lower concentrations, suggests a very high affinity of the pEA $\beta$ (3-42) peptide for its fibril surfaces, leading to saturation of the binding sites on the fibril surfaces already at lower concentrations, and hence to a weaker concentration dependence.





**Fig. 2** Interaction of pEA $\beta$ (3-42) and A $\beta$ (1-42) monomers. (A) Aggregation kinetics of A $\beta$ (1-42), pEA $\beta$ (3-42) and mixtures of both peptides measured by ThT assay. (B) Half-times of A $\beta$ (1-42), pEA $\beta$ (3-42) and mixtures of both determined from normalized aggregation kinetic data. The asterisk indicates that no aggregation could be detected. (C) Aggregation monitored by ThT assay of pEA $\beta$ (3-42) and A $\beta$ (1-42) below their critical concentration and mixtures of both. (D) Half-times of different concentrations of pEA $\beta$ (3-42) and A $\beta$ (1-42) mixtures plotted as a function of the total pEA $\beta$  percentage and fitted with an exponential function. (E) Coefficients of a fit of an exponential function to the decrease in half-time of pEA $\beta$ (3-42) and A $\beta$ (1-42) monomer mixtures plotted as a function of the total molarity. The solid lines are linear fits (red: slope  $-0.69 \pm 0.01$ , blue  $-0.07 \pm 0.03$ ) (F) normalized signal intensity gained from NMR spectroscopy time series of 10  $\mu\text{M}$  homomolecular pEA $\beta$ (3-42) or A $\beta$ (1-42). The dashed line marks 50% signal intensity and the red and blue bars indicate the times when half of the monomer of pEA $\beta$ (3-42) or A $\beta$ (1-42) was consumed. (G) Normalized intensity gained from NMR spectra monitoring monomer depletion of either 10  $\mu\text{M}$  pEA $\beta$ (3-42) or A $\beta$ (1-42), respectively, starting from equimolar mixtures and the percentage of A $\beta$ (1-42) monomers plotted against pEA $\beta$ (3-42) monomers (H).



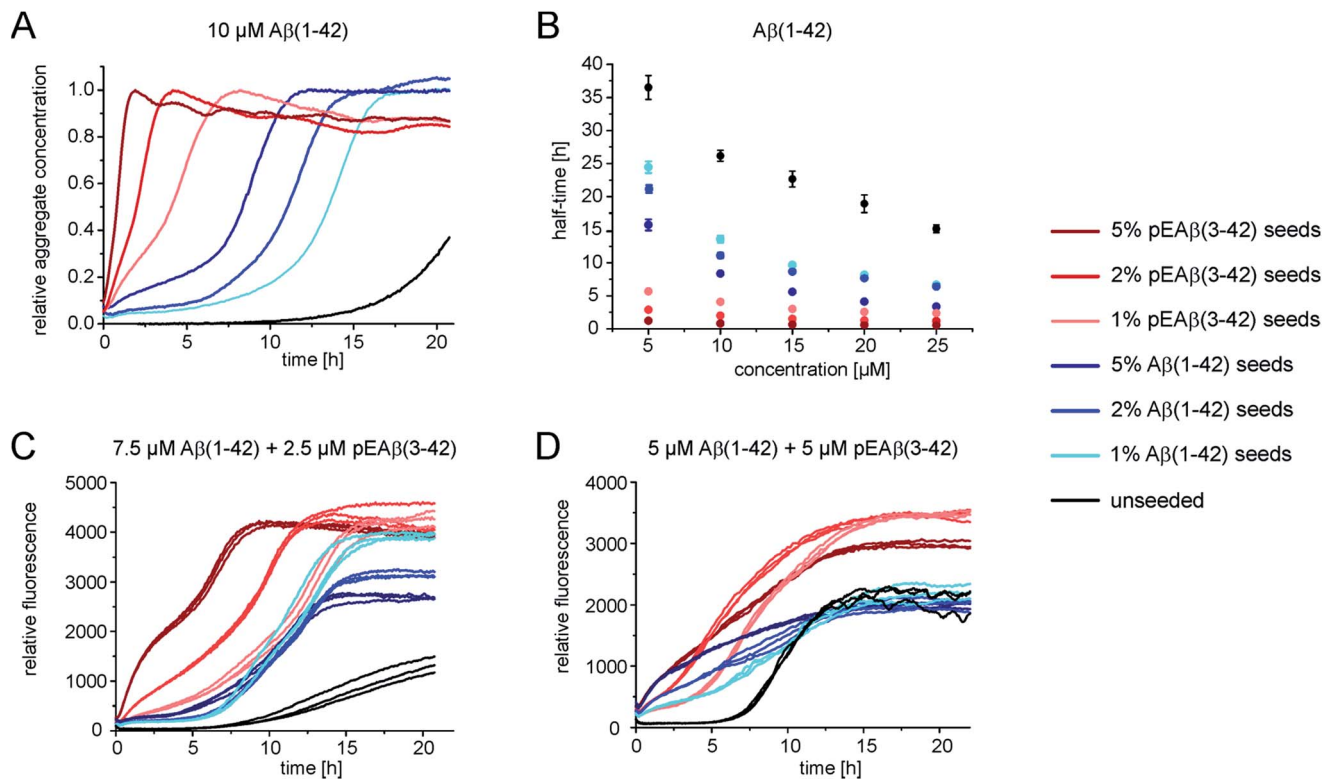


Fig. 3 Seeded aggregation kinetics of Aβ(1-42) monomers. (A) Normalized aggregation kinetics of 10 μM Aβ(1-42) monomers, unseeded and seeded with different concentrations of Aβ(1-42) or pEAβ(3-42) fibrils and normalized according to the aggregate concentration. (B) Half-times of varying Aβ(1-42) monomer concentrations seeded with different amounts of fibrils. (C) Aggregation kinetics of 7.5 μM Aβ(1-42) and 2.5 μM pEAβ(3-42) and of equimolar 5 μM Aβ(1-42) and pEAβ(3-42) (D) seeded with Aβ(1-42) and pEAβ(3-42) fibrils in varying concentrations.

### pEAβ(3-42) and Aβ(1-42) monomers co-aggregate

In order to obtain further insight into the origin of the faster aggregation of pEAβ(3-42) compared to Aβ(1-42), the aggregation kinetics of pure peptide were compared with those of mixtures of varying composition and total concentration (Fig. 2A and B and S2†).

Heteromolecular mixtures of monomeric pEAβ(3-42) and Aβ(1-42) displayed a single sigmoidal aggregation kinetic curve, indicating that both species undergo co-aggregation. The half-times, which are determined as the times when half of the final aggregate mass was reached, were calculated and compared with the kinetics of homomolecular aggregation of pEAβ(3-42) or Aβ(1-42), respectively (Fig. 2B). The half-times of the mixtures increase significantly with increasing Aβ(1-42) concentration, compared to the aggregation of pure pEAβ(3-42), even when Aβ(1-42) is added at a concentration where it does not display aggregation on its own.

In addition, amyloid fibril formation is also observed in mixtures of both species at concentrations of Aβ(1-42) (2 μM) and pEAβ(3-42) (0.5 μM) where each of the species individually does not show any aggregation under the same conditions (Fig. 2C). This finding further supports the hypothesis that the two species interact already at the level of the primary nucleation step.

The aggregation kinetics of different monomeric mixtures of Aβ(1-42) and pEAβ(3-42), varying from 0% to 100% of pEAβ(3-

42) at total concentrations from 5 to 25 μM were analysed. The data were normalised, the half-times were calculated and plotted as a function of the proportion of pEAβ(3-42) concentration for each total concentration set that had been measured (Fig. 2D). In order to be able to quantify the differences between the individual data sets, we fitted the decrease in half-time as a function of the proportion of pEAβ(3-42) with a single exponential function. We would like to stress that this does not imply that the underlying functional behaviour is necessarily exponential, but an exponential function yielded the best fit results. The exponents from the fits (numerical values are shown in Table S1†) were then plotted as a function of the total concentration from 10 to 25 μM (Fig. 2E). The results show, that the higher the total peptide concentration, the smaller the percentage of pEAβ(3-42) needed to significantly decrease the aggregation half-times, suggesting that the absolute concentration of pEAβ(3-42) is important for the accelerating effect. Two approximately linear regimes were observed, intersecting at a total concentration around 10 μM, which was shown to be the concentration where the surface-dependent secondary nucleation of Aβ(1-40) becomes saturated and hence concentration independent.<sup>34</sup> This change in behaviour suggests that the mechanism of co-aggregation of both species varies as a function of the total Aβ concentration. The finding that the accelerating effect of pEAβ(3-42) is more pronounced at higher concentrations (above 10 μM), where secondary nucleation is





likely to be concentration independent due to saturation (see above) suggests that the predominant process responsible for the acceleration at these higher concentrations is primary nucleation. The rate of primary nucleation cannot be saturated and hence does not show a concentration-independent regime.

### Monomer depletion of pEA $\beta$ (3-42) and A $\beta$ (1-42) monitored during co-nucleation

As ThT assays are almost exclusively sensitive to the formation of fibrillar species, we decided to also monitor the evolution of the concentration of monomeric A $\beta$  *via* nuclear magnetic resonance (NMR) spectroscopy, based on the invisibility in conventional NMR experiments of large aggregated species.<sup>35</sup> The monomer depletion of either A $\beta$ (1-42) or pEA $\beta$ (3-42) as homomolecular samples are complementary to the ThT aggregation kinetics (Fig. 2F). An experiment with a starting concentration of 10  $\mu$ M A $\beta$ (1-42) shows that half the peptide has become insoluble after 23 h and reaches a minimum in signal intensity at 27.5 h. In contrast, soluble pEA $\beta$ (3-42) monomers have decreased to 50% of the initial concentration after 4 h and the signal has almost completely disappeared after 5 h. Interestingly, in equimolar mixtures with the same concentrations of pEA $\beta$ (3-42) and A $\beta$ (1-42), the time courses of monomer depletion of both species differ significantly from those obtained from experiments with pure peptides (Fig. 2G). In this mixture, the loss of soluble A $\beta$ (1-42) is faster than in a pure sample of A $\beta$ (1-42), whereas the loss of soluble pEA $\beta$ (3-42) is slower than in the pure case, providing additional support for the hypothesis that both species interact with each other throughout the time course of aggregation. The concentration of monomeric pEA $\beta$ (3-42) decreases faster than that of A $\beta$ (1-42) monomers (Fig. 2F and G). Although pEA $\beta$ (3-42) and A $\beta$ (1-42) show different half-times, both NMR signal intensities are minimal after 25 h, indicating the formation of mixed aggregates up to the end of the aggregation reaction. Plotting the A $\beta$ (1-42) monomer concentration as a function of the pEA $\beta$ (3-42) monomer concentration illustrates that the A $\beta$ (1-42) monomer concentration stays close to its initial value until the pEA $\beta$ (3-42) concentration has decreased to approximately 50% (Fig. 2H). Thus, the aggregation of A $\beta$ (1-42) is accelerated most strongly in the presence of pEA $\beta$ (3-42) fibrils indicating that fibrils of pEA $\beta$ (3-42) provide efficient nucleation sites for A $\beta$ (1-42) monomers.

### pEA $\beta$ (3-42) fibrils as a highly catalytic surface for secondary pathways

In order to gain further insight into the role of aggregates in the mechanism of co-aggregation, we performed kinetic assays with preformed seed fibrils that can act as templates for elongation and as catalytic surfaces for secondary nucleation. Experiments with A $\beta$ (1-42) monomers showed that pEA $\beta$ (3-42) fibrils are very efficient seeds for these monomers (Fig. 3A and S3†). At high pEA $\beta$ (3-42) seed concentration (5%) A $\beta$ (1-42) aggregation is dominated by elongation, as evidenced by the concave aggregation time course, whereas the aggregation curves at lower seed concentrations show the typical convex shape indicative of

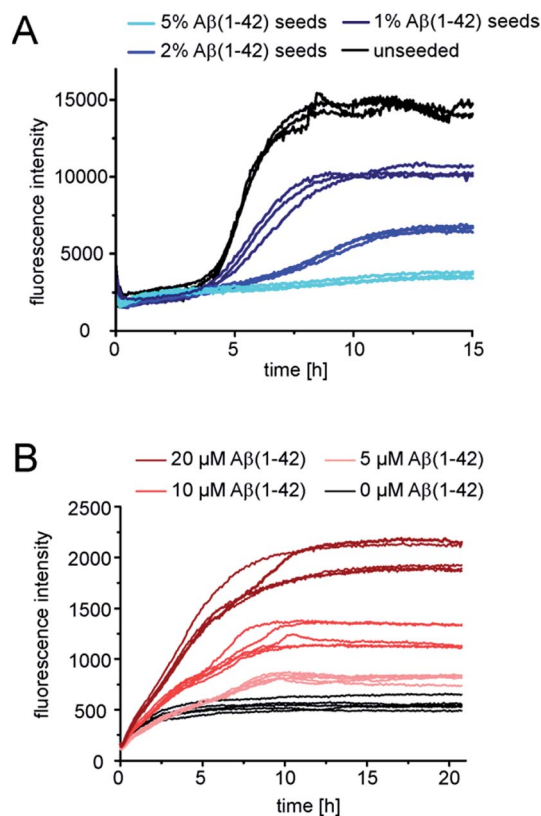


Fig. 4 Seeded kinetic assays of pEA $\beta$ (3-42) monomers. (A) Aggregation kinetics of 2.5  $\mu$ M pEA $\beta$ (3-42) unseeded and seeded with varying concentrations of A $\beta$ (1-42) fibrils. (B) Aggregation kinetics of 5  $\mu$ M pEA $\beta$ (3-42) seeded with 20% pEA $\beta$ (3-42) fibrils and additional A $\beta$ (1-42) monomers in varying concentrations.

an accelerating aggregation reaction and hence of the contribution of secondary processes.<sup>36</sup> Compared to the seeding effect of A $\beta$ (1-42) fibrils, only small amounts of pEA $\beta$ (3-42) fibrils are needed to accelerate A $\beta$ (1-42) aggregation drastically, and this accelerating effect is only weakly dependent on the total initial concentration of monomeric A $\beta$ (1-42) as shown by analysis of the half-times (Fig. 3B). Without a complete kinetic analysis of the co-aggregating system, it is difficult to quantify the relative contributions of elongation and secondary nucleation to the highly efficient seeding by pEA $\beta$ (3-42) fibrils. A higher elongation rate could for example be caused simply by the larger number of growth-competent ends per unit mass of fibrils, as the pEA $\beta$ (3-42) fibrils are on average shorter (Fig. 1C). Furthermore, differences in elongation or indeed secondary nucleation rate could also be caused by differences in the molecular structure of the fibrils, both at the ends and on the surface. The experimental finding of a decreasing concentration dependence of the accelerating effect with increasing initial monomer concentration suggests that a potential contribution from secondary nucleation is saturating.

Interesting behaviour is observed when mixtures of monomeric A $\beta$ (1-42) and pEA $\beta$ (3-42) are seeded. Some of the kinetic curves are first concave, then convex and then concave again (Fig. 3C and D), in particular those reactions that were seeded



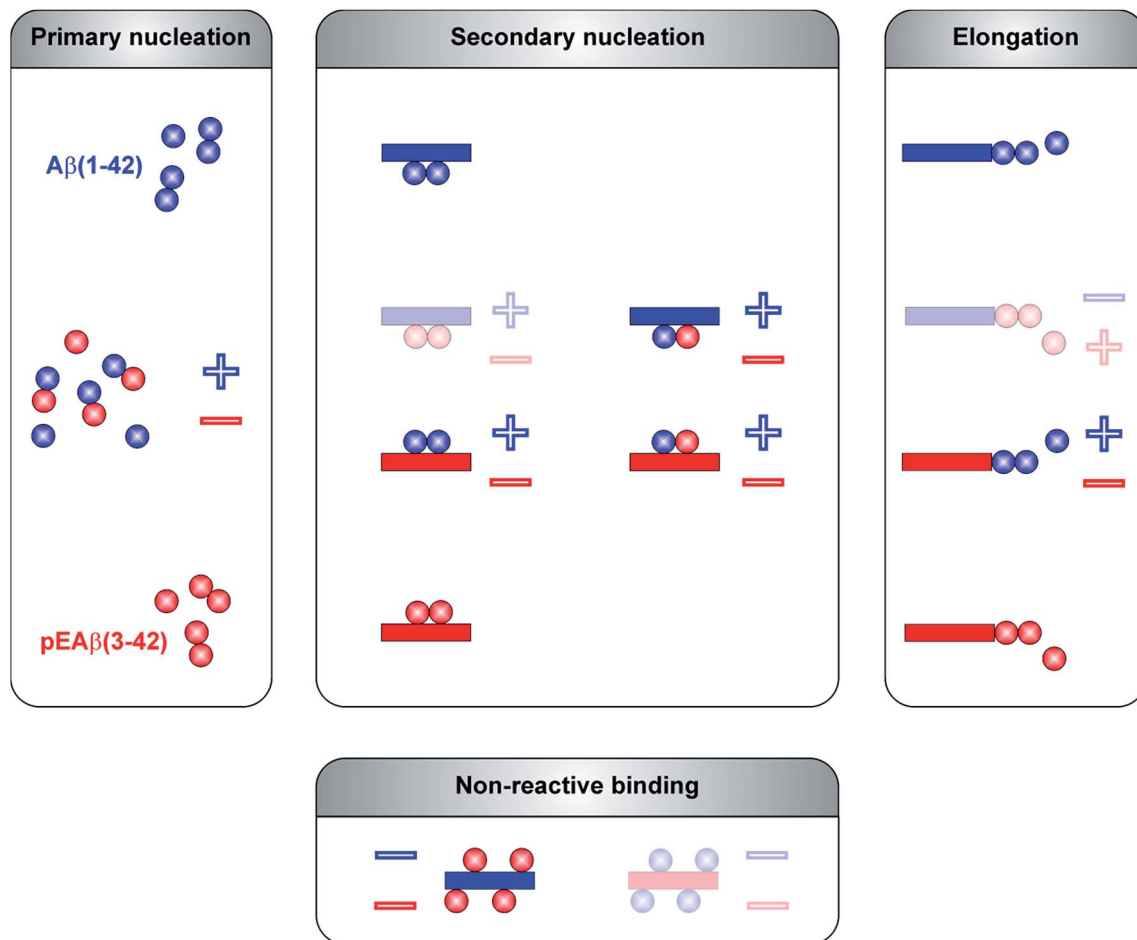


Fig. 5 Reaction scheme of molecular processes during A $\beta$  oligomerization and aggregation. Microscopic events of A $\beta$ (1-42) are displayed in blue and in red for pEA $\beta$ (3-42). Interactions are separated between primary pathways and secondary pathways as well as non-reactive binding. Individual steps which are accelerated in the presence of the other A $\beta$  species are marked with a plus and with a minus in case of a decelerating effect. Molecular events which can be excluded based on our data are shown as faded schemes.

with pEA $\beta$ (3-42). This resembles the unseeded aggregation curves that have been reported for mixtures of the A $\beta$ (1-42) and A $\beta$ (1-40) peptides,<sup>28</sup> which were shown not to co-aggregate significantly. However, the results of our unseeded kinetic experiments by ThT and NMR of mixtures of A $\beta$ (1-42) and pEA $\beta$ (3-42) (Fig. 2C and G and black curves in Fig. 3A, C and D) do not show biphasic behaviour and present clear evidence for co-aggregation. The biphasic aggregation curves in the presence of seeds can therefore be explained through a preferential incorporation of one type of soluble A $\beta$  into the seed aggregates, followed by the slower and less efficient incorporation of the remaining monomer type. The later acceleration in aggregation rate is then likely to be due to secondary nucleation of the remaining soluble A $\beta$  on the surface of the mixed fibrils. This phenomenon is observed in monomer mixtures containing a molar excess of A $\beta$ (1-42), *e.g.* 7.5  $\mu$ M A $\beta$ (1-42) and 2.5  $\mu$ M pEA $\beta$ (3-42) monomers (Fig. 3C).

The two-phase kinetic behaviour is less pronounced in equimolar mixtures, when the total amount of pEA $\beta$ (3-42) monomers is increased (Fig. 3D). At equimolar ratio the direct interaction of pEA $\beta$ (3-42) monomers with A $\beta$ (1-42) monomers is

likely to play a more pronounced role. This interaction, which leads to the formation of mixed primary nuclei, appears to weaken the difference between the effects of the two types of fibrils, as the initial slopes are very similar until secondary nucleation becomes manifest through an increase in the aggregation rate. Both types of seeds lead to very similar initial aggregation rates under those conditions, that only depend on the total fibril mass, but the reactions that were seeded with pEA $\beta$ (3-42) fibrils subsequently show a clear increase in rate, indicative of rapid secondary nucleation. This finding suggests that the structural features of the pEA $\beta$ (3-42) fibrils render their surfaces more amenable to secondary nucleation.

Overall, this data is consistent with an incorporation of A $\beta$ (1-42) into pEA $\beta$ (3-42) seeds that is more efficient than the incorporation of pEA $\beta$ (3-42), *i.e.* heteromolecular elongation is more efficient than homomolecular elongation. This unexpected behaviour is for example suggested by the more rapid aggregation in Fig. 3A compared to Fig. 3C (red curves). It has to be noted, however, that seeded aggregation experiments need to be compared with care, as the aggregation rate depends on the concentration of growth-competent seeds, which is difficult to



control and determine precisely, as it is a function of the exact length distribution of the seeds.

In order to obtain insight into the structural consequences of the complex interaction behaviour described above, we have acquired atomic force microscopy (AFM) and transmission electron microscopy (TEM) images of mixtures of 5  $\mu\text{M}$  pEA $\beta$ (3-42) and 5  $\mu\text{M}$  A $\beta$ (1-42) that were either unseeded, seeded with 5% pEA $\beta$ (3-42) fibrils or with 5% A $\beta$ (1-42) fibrils (Fig. S4†). These images show that in each case, long fibrils and smaller species coexist.

Elucidation of the full mechanism of coaggregation as a function of seed type and concentration, as well as monomer ratio and concentration, requires a systematic and comprehensive imaging study, combined with a determination of the ratio of soluble peptides as a function of time for each of these conditions, which will be the subject of a future study.

### A $\beta$ (1-42) fibrils are not suitable for cross-seeding of pEA $\beta$ (3-42)

Next we tested whether A $\beta$ (1-42) fibrils are able to seed pure monomeric pEA $\beta$ (3-42). Aggregation kinetics of pEA $\beta$ (3-42) monomers was delayed even in the presence of 1% A $\beta$ (1-42) fibrils and the total aggregate mass (as deduced from fluorescence intensity) was decreased (Fig. 4A) compared to the unseeded case. By adding 5% A $\beta$ (1-42) fibrils the fibrillation of pEA $\beta$ (3-42) was almost completely inhibited, as judged by ThT fluorescence. This phenomenon is dependent on the A $\beta$ (1-42) fibril concentration and was also observed for equimolar mixtures of both monomeric species. Aggregation is inhibited and decreased if the amount of A $\beta$ (1-42) fibrils is large enough, *i.e.* 20% (Fig. S5†). This result suggests that pEA $\beta$ (3-42) monomers can attach to the A $\beta$ (1-42) fibril surface in a way that does not allow secondary nucleation. In order to further support this hypothesis, we performed NMR experiments, whereby we measured the decrease in NMR signal of soluble pEA $\beta$ (3-42) upon addition of 5% A $\beta$ (1-42) (Fig. S6†). Within the time scale of the NMR experiment (*ca.* 10 min), we observe a very significant (*ca.* 50%) decrease in signal intensity, suggesting that half of the soluble pEA $\beta$ (3-42) peptide strongly interacts with the A $\beta$ (1-42) fibrils, with a very high stoichiometry of the order of 10 : 1. We have acquired AFM images of a mixture of pEA $\beta$ (3-42) and 5% A $\beta$ (1-42) fibrils (Fig. S7†) that show clusters of fibrils that appear to be coated in monomer. Thus, we conclude that pEA $\beta$ (3-42) binds with a high affinity, as well as stoichiometry, to A $\beta$ (1-42) fibrils, and this interaction does not lead to self-replication through secondary nucleation.

Non-reactive surface binding and thus the absence of self-replication of amyloidogenic peptides was recently postulated, based on the results of coarse-grained simulations.<sup>37</sup> The overall reaction rate of secondary nucleation was shown to be determined by the protein adsorption and subsequent oligomer formation on the fibril surface, the latter being only possible at intermediate protein-fibril interaction strengths. Too strong interactions render the surface-bound peptides inert.

Although A $\beta$ (1-42) monomers drastically decelerate pEA $\beta$ (3-42) primary and secondary nucleation, the pEA $\beta$ (3-42) elongation

rate, as evaluated from the initial slope of the aggregation curve, is not significantly affected as demonstrated in the presence of high amounts of pEA $\beta$ (3-42) fibrils (Fig. 4B and S8†). This suggests that the rates of incorporation of both A $\beta$ (1-42) and pEA $\beta$ (3-42) into pEA $\beta$ (3-42) fibrils are not substantially different and that therefore the latter provide an efficient template for elongation of both types of peptide, whereas A $\beta$ (1-42) fibrils can only act as homomolecular templates.

## Conclusions

The aggregation mechanism of A $\beta$ (1-42) was previously shown to be secondary nucleation dominated under quiescent conditions.<sup>25–27</sup> In contrast to C-terminally truncated A $\beta$  species which aggregate into homofibrils without co-nucleation,<sup>28</sup> N-terminal modifications are able to co-aggregate.<sup>29</sup> Here, we have elucidated the mechanism of co-aggregation of A $\beta$ (1-42) with the more toxic and the more aggregation prone variant pEA $\beta$ (3-42) and our results are summarized schematically in Fig. 5. The presence of small amounts of pEA $\beta$ (3-42) monomers increases the primary nucleation rate of A $\beta$ (1-42) and pEA $\beta$ (3-42) fibrils serve as highly efficient seeds for both elongation and (auto)catalytic secondary nucleation of non-N-terminally truncated A $\beta$  monomers while pEA $\beta$ (3-42) aggregation itself is slowed down through the presence of A $\beta$ (1-42) monomers. In addition, A $\beta$ (1-42) fibrils are not suitable as templates for the incorporation of monomeric pEA $\beta$ (3-42) but can even prevent pEA $\beta$ (3-42) aggregation at high fibril concentrations, presumably due to the non-reactive binding of pEA $\beta$ (3-42) monomers to A $\beta$ (1-42) fibril surfaces. Thus, pEA $\beta$ (3-42) catalyses aggregation of A $\beta$ (1-42) affecting all reaction processes while A $\beta$ (1-42) dramatically slows down pEA $\beta$ (3-42) primary and secondary pathways by non-reactive surface binding. Therefore, the presence of even relatively small amounts of additional isoforms can very significantly change the aggregation behavior of the A $\beta$ (1-42) peptide. The insight gained in this study will enable a more detailed understanding of the aggregation dynamics *in vivo*, where complex mixtures of various isoforms of the A $\beta$  peptide are likely to be present.

## Methods

### Recombinant A $\beta$ peptides

Expression and purification of pEA $\beta$ (3-42) was performed as described recently.<sup>30</sup> Briefly, A $\beta$ (E3Q-42) was expressed in *E. coli* BL21 (DE3) pLysS as a fusion protein and purified *via* immobilized metal affinity chromatography (IMAC) and reversed-phase high performance liquid chromatography (RP-HPLC). The fusion-tag was cleaved by tobacco etch virus (TEV) protease and RP-HPLC purified A $\beta$ (E3Q-42) was non-enzymatically converted to pEA $\beta$ (3-42) under mild acidic conditions. Final pEA $\beta$ (3-42) was obtained in purities of  $\geq 98\%$ . Recombinant A $\beta$ (1-42) was purchased from Isoloid (Düsseldorf, Germany).

### Sample preparation

Samples were prepared in Protein LowBinding tubes (Eppendorf AG, 230 Hamburg, Germany). The purified A $\beta$  peptides



were dissolved in 1,1,1,3,3,3-hexafluoro-2-propanol (HFIP, Sigma-Aldrich, Hannover, Germany), incubated for 3 days at room temperature for disaggregation. Monomerised peptides were lyophilized directly from HFIP and stored at room temperature. Prior to use, purified peptides were again dissolved in HFIP, monomerised overnight and final sample aliquots were prepared and lyophilized.

### Preparation of fibrils

Lyophilized pEA $\beta$ (3-42) and A $\beta$ (1-42) were dissolved in 10 mM sodium phosphate buffer pH 7.4 to a final protein concentration of 50  $\mu$ M, respectively, and incubated at 37 °C for seven days without agitation.

### Kinetic assays of monomers

A $\beta$ (1-42) and pEA $\beta$ (3-42) dissolved in HFIP were aliquoted, lyophilized and directly dissolved in 10 mM ice-cold sodium phosphate buffer pH 7.4 including 10  $\mu$ M ThT. The solutions were vortexed; dilutions series were prepared and gently mixed by pipetting up and down. The final concentration of prepared samples was ranging between 0.5  $\mu$ M and 25  $\mu$ M, depending on the peptide. Aggregation assays were performed in black non-binding 96-well plates (Sigma-Aldrich, Germany) with 100  $\mu$ L per well as triplicates at 37 °C in quiescent conditions. Fluorescence was monitored using a microplate reader (PolarStar Optima, BMG, Offenburg, Germany) with 440 and 492 nm excitation and emission filters, respectively, in bottom-read mode.

### Kinetic assays of monomer mixtures

Monomer mixtures of A $\beta$ (1-42) and pEA $\beta$ (3-42) were prepared with stock solutions dissolved in HFIP, respectively, mixed in reaction tubes and lyophilized prior to use. Mixed monomers were dissolved in 10 mM ice-cold sodium phosphate buffer pH 7.4 including 10  $\mu$ M ThT, vortexed and sonicated for 2 min and dilutions series were prepared. The final concentrations of the mixtures were in a range of 0.5 to 25  $\mu$ M. Aggregation assays were performed in triplicates as described above.

### Seeded kinetic assays

Samples for seeded kinetic assays of A $\beta$ (1-42) and pEA $\beta$ (3-42) monomer homogenates as well as mixtures were prepared as described above and dissolved in ice-cold 10 mM sodium phosphate pH 7.4 and 10  $\mu$ M ThT. Fibrils were sonicated for 2 min prior to use and added to the reaction tube in final concentrations of 1, 2 or 5% in monomer equivalents. Dilution series were prepared and concentrations of final samples were ranging from 0.5  $\mu$ M to 25  $\mu$ M with 1, 2 or 5% seeds. Aggregation assays were performed in triplicates as described above.

### Analysis of aggregation kinetics

Analysis of homomolecular A $\beta$ (1-42) and pEA $\beta$ (3-42) aggregation kinetics was performed using the online tool AmyloFit published by Meisl, Knowles and coworkers.<sup>31</sup> Briefly, kinetic datasets were normalized to their final aggregate concentration,

plotted as a function of time and fitted using the appropriate model.<sup>32,33</sup> Heteromolecular data could not be analysed *via* this tool as multiple processes occurred during aggregation. This data was analysed either by plotting raw or normalized data and especially halftimes; the point where aggregation has reached half its maximum.

### TEM

Fibrils were absorbed on formvar/carbon coated copper grids (S162, Plano, Wetzlar, Germany) for 5 min and washed with water. Negative staining was performed by incubation with 2% (w/v) uranylacetate for 45 s. Images were taken with a Libra 120 transmission electron microscope (Zeiss, Oberkochen, Germany) at 120 kV.

### NMR spectroscopy

Lyophilized natural abundant pEA $\beta$ (3-42) and [ $^{13}$ C,  $^{15}$ N]-A $\beta$ (1-42) as well as equimolar mixtures were dissolved in 10 mM sodium phosphate buffer pH 7.4 including 5% D<sub>2</sub>O to a final protein concentration of 10  $\mu$ M of each A $\beta$  species. Titration experiments were performed by dissolving pEA $\beta$ (3-42) to a final concentration of 5  $\mu$ M. A $\beta$ (1-42) fibrils were then directly added. NMR spectra were acquired using a Varian 800 MHz or a Bruker 700 MHz spectrometer equipped with cryogenically cooled z-pulse-field-gradient probes at 37 °C. Methyl-proton signals were obtained from CN-filtered-noesy,<sup>38</sup> gChsqc<sup>39</sup> or zgpr pulse sequences, respectively. Spectra were processed with NMRPipe<sup>40</sup> and evaluated with CCPNmr Analysis.<sup>41</sup>

## Acknowledgements

We thank Gunnar Schröder, Matthias Stoldt, Lothar Gremer, Nicola Vettore and Tamar Ziehm for assistance and discussions. The authors acknowledge access to the Jülich-Düsseldorf Biomolecular NMR Center. DW was supported by grants from the "Portfolio Technology and Medicine", the "Portfolio Drug Research" and the Helmholtz-Validierungsfonds of the Impuls und Vernetzung-Fonds der Helmholtzgemeinschaft. AKB thanks the Alzheimer Forschung Initiative (AFI) for support.

## Notes and references

- X. Hu, S. L. Crick, G. Bu, C. Frieden, R. V. Pappu and J. M. Lee, *Proc. Natl. Acad. Sci. U. S. A.*, 2009, **106**, 20324–20329.
- A. Aguzzi and T. O'Connor, *Nat. Rev. Drug Discovery*, 2010, **9**, 237–248.
- L. N. Zhao, L. Lu, L. Y. Chew and Y. Mu, *Int. J. Mol. Sci.*, 2014, **15**, 12631–12650.
- Y. Harigaya, T. C. Saido, C. B. Eckman, C. M. Prada, M. Shoji and S. G. Younkin, *Biochem. Biophys. Res. Commun.*, 2000, **276**, 422–427.
- S. Jawhar, O. Wirhth and T. A. Bayer, *J. Biol. Chem.*, 2011, **286**, 38825–38832.
- A. P. Gunn, C. L. Masters and R. A. Cherny, *Int. J. Biochem. Cell Biol.*, 2010, **42**, 1915–1918.





- 7 T. C. Saido, T. Iwatsubo, D. M. Mann, H. Shimada, Y. Ihara and S. Kawashima, *Neuron*, 1995, **14**, 457–466.
- 8 T. C. Saido, W. Yamao-Harigaya, T. Iwatsubo and S. Kawashima, *Neurosci. Lett.*, 1996, **215**, 173–176.
- 9 S. Schilling, T. Lauber, M. Schaupp, S. Manhart, E. Scheel, G. Bohm and H. U. Demuth, *Biochemistry*, 2006, **45**, 12393–12399.
- 10 N. Sun, R. Hartmann, J. Lecher, M. Stoldt, S. A. Funke, L. Gremer, H. H. Ludwig, H. U. Demuth, M. Kleinschmidt and D. Willbold, *J. Pept. Sci.*, 2012, **18**, 691–695.
- 11 C. Dammers, L. Gremer, K. Reiss, A. N. Klein, P. Neudecker, R. Hartmann, N. Sun, H. U. Demuth, M. Schwarten and D. Willbold, *PLoS one*, 2015, **10**, e0143647.
- 12 R. Hosoda, T. C. Saido, L. Otvos Jr, T. Arai, D. M. Mann, V. M. Lee, J. Q. Trojanowski and T. Iwatsubo, *J. Neuropathol. Exp. Neurol.*, 1998, **57**, 1089–1095.
- 13 W. Hartig, S. Goldhammer, U. Bauer, F. Wegner, O. Wirths, T. A. Bayer and J. Grosche, *J. Chem. Neuroanat.*, 2010, **40**, 82–92.
- 14 C. P. Sullivan, E. A. Berg, R. Elliott-Bryant, J. B. Fishman, A. C. McKee, P. J. Morin, M. A. Shia and R. E. Fine, *Neurosci. Lett.*, 2011, **505**, 109–112.
- 15 J. Naslund, A. Schierhorn, U. Hellman, L. Lannfelt, A. D. Roses, L. O. Tjernberg, J. Silberring, S. E. Gandy, B. Winblad, P. Greengard, *et al.*, *Proc. Natl. Acad. Sci. U. S. A.*, 1994, **91**, 8378–8382.
- 16 W. He and C. J. Barrow, *Biochemistry*, 1999, **38**, 10871–10877.
- 17 D. Schlenzig, R. Ronicke, H. Cynis, H. H. Ludwig, E. Scheel, K. Reymann, T. Saido, G. Hause, S. Schilling and H. U. Demuth, *J. Neurochem.*, 2012, **121**, 774–784.
- 18 C. D'Arrigo, M. Tabaton and A. Perico, *Biopolymers*, 2009, **91**, 861–873.
- 19 K. Brannstrom, A. Ohman, L. Nilsson, M. Pihl, L. Sandblad and A. Olofsson, *J. Am. Chem. Soc.*, 2014, **136**, 10956–10964.
- 20 M. Wulff, M. Baumann, A. Thummler, J. K. Yadav, L. Heinrich, U. Knupfer, D. Schlenzig, A. Schierhorn, J. U. Rahfeld, U. Horn, J. Balbach, H. U. Demuth and M. Fandrich, *Angew. Chem., Int. Ed.*, 2016, **55**, 5081–5084.
- 21 H. Cynis, J. L. Frost, H. Crehan and C. A. Lemere, *Mol. Neurodegener.*, 2016, **11**, 48.
- 22 E. Niederwolfgruber, T. L. Schmitt, I. Blasko, K. Trieb, M. M. Steger, C. Maczek, J. Hager, K. Bobak, E. Steiner and B. Grubeck-Loebenstien, *J. Gerontol., Ser. A*, 1998, **53**, B186–B190.
- 23 C. Haass, M. G. Schlossmacher, A. Y. Hung, C. Vigo-Pelfrey, A. Mellon, B. L. Ostaszewski, I. Lieberburg, E. H. Koo, D. Schenk, D. B. Teplow, *et al.*, *Nature*, 1992, **359**, 322–325.
- 24 J. L. Frost, B. Liu, J. U. Rahfeld, M. Kleinschmidt, B. O'Nuallain, K. X. Le, I. Lues, B. J. Caldarone, S. Schilling, H. U. Demuth and C. A. Lemere, *Neurobiol. Aging*, 2015, **36**, 3187–3199.
- 25 S. I. Cohen, S. Linse, L. M. Luheshi, E. Hellstrand, D. A. White, L. Rajah, D. E. Otzen, M. Vendruscolo, C. M. Dobson and T. P. Knowles, *Proc. Natl. Acad. Sci. U. S. A.*, 2013, **110**, 9758–9763.
- 26 P. Arosio, T. P. Knowles and S. Linse, *Phys. Chem. Chem. Phys.*, 2015, **17**, 7606–7618.
- 27 P. Arosio, R. Cukalevski, B. Frohm, T. P. Knowles and S. Linse, *J. Am. Chem. Soc.*, 2014, **136**, 219–225.
- 28 R. Cukalevski, X. T. Yang, G. Meisl, U. Weininger, K. Bernfur, B. Frohm, T. P. J. Knowles and S. Linse, *Chem. Sci.*, 2015, **6**, 4215–4233.
- 29 O. Szczepankiewicz, B. Linse, G. Meisl, E. Thulin, B. Frohm, C. Sala Frigerio, M. T. Colvin, A. C. Jacavone, R. G. Griffin, T. Knowles, D. M. Walsh and S. Linse, *J. Am. Chem. Soc.*, 2015, **137**, 14673–14685.
- 30 C. Dammers, L. Gremer, P. Neudecker, H. U. Demuth, M. Schwarten and D. Willbold, *PLoS one*, 2015, **10**, e0139710.
- 31 G. Meisl, J. B. Kirkegaard, P. Arosio, T. C. Michaels, M. Vendruscolo, C. M. Dobson, S. Linse and T. P. Knowles, *Nat. Protoc.*, 2016, **11**, 252–272.
- 32 S. I. Cohen, M. Vendruscolo, C. M. Dobson and T. P. Knowles, *J. Chem. Phys.*, 2011, **135**, 065107.
- 33 T. P. Knowles, C. A. Waudby, G. L. Devlin, S. I. Cohen, A. Aguzzi, M. Vendruscolo, E. M. Terentjev, M. E. Welland and C. M. Dobson, *Science*, 2009, **326**, 1533–1537.
- 34 G. Meisl, X. Yang, E. Hellstrand, B. Frohm, J. B. Kirkegaard, S. I. Cohen, C. M. Dobson, S. Linse and T. P. Knowles, *Proc. Natl. Acad. Sci. U. S. A.*, 2014, **111**, 9384–9389.
- 35 N. J. Anthis and G. M. Clore, *Q. Rev. Biophys.*, 2015, **48**, 35–116.
- 36 S. I. Cohen, M. Vendruscolo, C. M. Dobson and T. P. Knowles, *Int. J. Mol. Sci.*, 2011, **12**, 5844–5852.
- 37 A. Saric, A. K. Buell, G. Meisl, T. C. Michaels, C. M. Dobson, S. Linse, T. Knowles and D. Frenkel, *Nat. Phys.*, 2016, **12**, 874–880.
- 38 C. Zwahlen, P. Legault, S. J. F. Vincent, J. Greenblatt, R. Konrat and L. E. Kay, *J. Am. Chem. Soc.*, 1997, **119**, 6711–6721.
- 39 L. E. Kay, P. Keifer and T. Saarinen, *J. Am. Chem. Soc.*, 1992, **114**, 10663–10665.
- 40 F. Delaglio, S. Grzesiek, G. W. Vuister, G. Zhu, J. Pfeifer and A. Bax, *J. Biomol. NMR*, 1995, **6**, 277–293.
- 41 W. F. Vranken, W. Boucher, T. J. Stevens, R. H. Fogh, A. Pajon, M. Llinas, E. L. Ulrich, J. L. Markley, J. Ionides and E. D. Laue, *Proteins*, 2005, **59**, 687–696.

